

# Effective slip and friction reduction in nanograted superhydrophobic microchannels

Chang-Hwan Choi,<sup>a)</sup> Umberto Ulmanella,<sup>b)</sup> Joonwon Kim,<sup>c)</sup>  
Chih-Ming Ho, and Chang-Jin Kim

Department of Mechanical and Aerospace Engineering, University of California at Los Angeles,  
Los Angeles, California 90095-1597

(Received 21 January 2006; accepted 20 July 2006; published online 24 August 2006)

Enabled by a technology to fabricate well-defined nanogrates over a large area ( $2 \times 2 \text{ cm}^2$ ), we report the effect of such a surface, in both hydrophilic and hydrophobic conditions, on liquid slip and the corresponding friction reduction in microchannels. The grates are designed to be dense ( $\sim 230 \text{ nm}$  pitch) but deep ( $\sim 500 \text{ nm}$ ) in order to sustain a large amount of air in the troughs when the grates are hydrophobic, even under pressurized liquid flow conditions (e.g., more than 1 bar). A noticeable slip (i.e., slip length of  $100\text{--}200 \text{ nm}$ , corresponding to  $20\%\text{--}30\%$  reduction of pressure drop in a  $\sim 3 \mu\text{m}$  high channel) is observed for water flowing parallel over the hydrophobic nanogrates; this is believed to be an “effective” slip generated by the nanostrips of air in the grate troughs under the liquid. The effective slip is clearer and larger in flows parallel to the nanograting patterns than in transverse, suggesting that the nanograted superhydrophobic surfaces would not only reduce friction in liquid flows under pressure but also enable directional control of the slip. This paper is the first to use *nanoscale* grating patterns and to measure their effect on liquid flows in microchannels. © 2006 American Institute of Physics. [DOI: 10.1063/1.2337669]

## I. INTRODUCTION

Although the classical fluid-dynamic assumption of a “no-slip” boundary condition (i.e., relative zero flow velocity at a solid wall) is quite satisfactory in dealing with most viscous flow problems of continuum fluids, molecular dynamics simulations<sup>1–4</sup> have shown that a microscopic slip is possible, depending on several fluid-solid interfacial parameters. The slip has recently drawn more attention as miniaturization technologies have reached down to micro and nanometer scales, where surface effects are inherently more important and the deviation by the surface slip is no longer negligible. Slip of *liquid* at a solid wall is especially important to many engineering topics involving liquid-solid interfacial phenomena, such as lubrication, flows through porous media, liquid coating, and particle aggregation. A number of new studies have confirmed the existence of a liquid slip over certain solid surfaces, as summarized in recent reviews.<sup>5–7</sup> Although a few studies<sup>8,9</sup> have reported a slip over hydrophilic surfaces, many theoretical,<sup>10,11</sup> experimental,<sup>12–23</sup> and numerical<sup>24</sup> studies have reported that hydrophobic surfaces allow a noticeable slip ranging from nanometers to a micron in “slip length” (the linearly extrapolated distance *into* a solid surface at which a no-slip condition would hold true). Several reasons have been proposed for the slip over hydrophobic surfaces, including a molecular slip,<sup>10</sup> a decrease in the viscosity of the boundary layer,<sup>11</sup> the

small dipole moment of a polar liquid,<sup>23</sup> and a gas gap or nanobubbles at the liquid-surface interface.<sup>13,25–29</sup> In particular, it should be noted that rough or patterned hydrophobic surfaces, so-called “superhydrophobic” surfaces, have been shown to generate a large “effective” slip by making the liquid flow partially over a layer of air in between nonwetting surface structures.<sup>30–37</sup>

This large effective slip by the rough or patterned hydrophobic surfaces is potentially of great significance in engineering, including microfluidic systems commonly employing microchannels. Although significant drag reduction was reported using rough-textured hydrophobic surfaces,<sup>30–34</sup> there has not been a deliberate effort to *design* and *fabricate* a surface to verify the surface roughness effect on the liquid slip in the *nanoscale* (e.g., nanobubbles effect). Furthermore, there has been no effort to produce a meaningful effective slip for drag reduction under practical conditions, e.g., highly *pressurized* flows, which are frequently encountered in engineering practice. The hydrophobic surface created by a polymer coating<sup>30–32</sup> is *irregularly* rough and the fine grooves (i.e., cracks) formed on the rough surface are random in size and pattern, making it difficult to isolate the effect of trapped air and to utilize the effective slip in a controllable manner. On the other hand, the *microscale* pitches of surface structures fabricated by conventional microfabrication technology<sup>33,34</sup> limit the use of such a surface to cases of small liquid pressure (i.e., less than 5 kPa) only. For the practical use of the patterned hydrophobic surface, in order to maintain the effective slip even under high liquid pressure, surface structures of *nanoscale pitch* with a relatively large area of pattern coverage are desired. Although molecular dynamics simulations<sup>35,36</sup> demonstrate that a large effective slip and friction reduction can be obtained by a nanoscale peri-

<sup>a)</sup> Author to whom correspondence should be addressed. Telephone: (310) 825-3977. Fax: (310) 206-2302. Electronic mail: chchoi@ucla.edu

<sup>b)</sup> Present address: Applied Biosystems, Foster City, California 94404.

<sup>c)</sup> Present address: Mechanical Engineering Department, Pohang University of Science and Technology (POSTECH), Pohang, Gyungbuk 790-784, Korea.

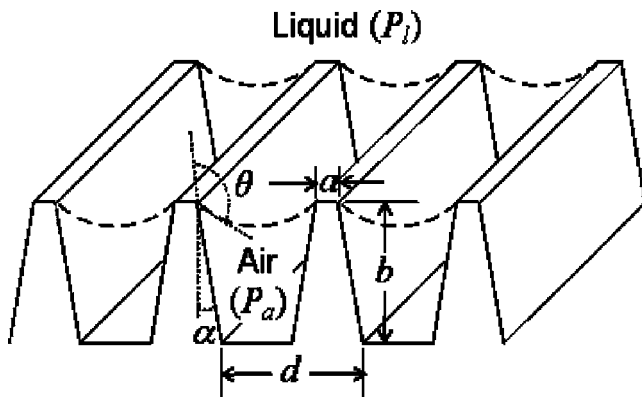


FIG. 1. Liquid meniscus expected over hydrophobic gratings. Grates with periodicity  $d$  have a cross section of a trapezoidal shape with height  $b$ , slope angle  $\alpha$ , and ridge width  $a$ . The meniscus has a cylindrical shape forming a contact angle  $\theta$  (or advancing contact angle  $\theta_A$  when the liquid pressure  $P_l$  increases) with the grate side. If  $P_l$  increases more than what the surface tension of the curved meniscus can balance, the meniscus would go down and liquid would fill the gap, causing the loss of levitation effect by the hydrophobic gratings. Grates with smaller periodicity can withstand higher liquid pressure before losing the levitation, an atmospheric pressure range calling for gratings with nanoscale periodicity.

odic pattern under certain pressurized flow conditions, there has been no experimental support to verify it. While our recent study,<sup>37</sup> extended from the prior achievement of low friction in discrete droplet movement,<sup>38</sup> has experimentally verified the concept of a large effective slip in continuous flows as well by using a nanoengineered superhydrophobic surface, the pattern and size of the surface structures were difficult to regulate and the tested flow condition was a non-pressurized Couette flow.

In this paper, we perform an experimental investigation on the effects of well-defined deep nanoperiodic line patterns (i.e., nanogratings), in both hydrophilic and hydrophobic surface conditions, upon the slip effect and friction reduction in highly pressurized liquid flows (e.g., more than 100 kPa). The effective slip and the corresponding reduction of pressure drop of water flow over the nanograting structures are measured in microchannel systems to represent a real engineering application. The regular nanograting patterns of  $\sim 230$  nm pitch with deep troughs ( $\sim 500$  nm) over a relatively large area ( $2 \times 2$  cm<sup>2</sup> for the current study) are enabled by a recently developed nanofabrication method<sup>39</sup> that couples interference lithography with deep reactive ion etching. The submicron periodicity is small enough to keep the pressurized liquid from filling the deep troughs of the hydrophobic nanogrates under most engineering practices, yet large enough to still consider the air as a continuum and to neglect the effect of wall potential.<sup>1-4</sup> Furthermore, the regularity of the surface patterns uniquely allows us to study the dependency of the slip effect on the orientation of the surface patterns: flows *parallel* and *transverse* to the patterns.

## II. MATERIALS AND METHODS

### A. Design of a superhydrophobic nanograted surface

Consider the liquid-air interface formed on hydrophobic grate patterns (Fig. 1). By a simple geometrical calculation

and the Laplace-Young equation, the grate spacing ( $d-a$ ) required to hold the liquid meniscus up against the liquid pressure over air  $\Delta P (=P_l - P_a)$  and the grate height  $b$  for the liquid meniscus not to touch the bottom surface can be obtained as

$$(d-a) < 2\sigma \frac{|\cos(\theta_A - \alpha)|}{\Delta P}, \quad b > \frac{1 - \sin(\theta_A - \alpha)}{2|\cos(\theta_A - \alpha)|}(d-a), \quad (1)$$

where  $\sigma$  is the surface tension of the liquid-air interface. A perfect quantitative agreement may not be expected with the idealized geometry in Fig. 1 because of the potential deviation from the conventional capillarity theory and the lack of fabrication precision in a submicron scale. However, Eq. (1) still serves as a key guideline in the design of proper grating geometry for the purpose at hand. For example, if the liquid is water ( $\sigma = 0.0727$  N/m at 20 °C),  $(\theta_A - \alpha)$  is 120° (e.g.,  $\theta_A = 130^\circ$  and  $\alpha = 10^\circ$ ), and  $\Delta P$  is 0.1 MPa (1 bar), which correspond to the material properties and test conditions of the present experiment, the grate spacing ( $d-a$ ) should be less than  $\sim 0.7$   $\mu\text{m}$ , and the grate height  $b$  should be larger than  $\sim 0.1$   $\mu\text{m}$ . This analysis indicates that the grating structures need to be relatively tall and populated on a submicron scale to produce the slip effects under realistic (i.e., pressure up to 1 bar range) conditions. The contradictory reports<sup>16,18</sup> that a molecular or a nanometer scale roughness strongly inhibits the slip even if the surface is hydrophobic may be explained by the possibility that the surface features in the studies are too small to trap air in a continuum sense and, hence, to exhibit the effective slip.

### B. Fabrication of nanograting structures

For the experiments, silicon nanograting patterns of  $\sim 230$  nm pitch ( $\sim 50$  nm ridge width and  $\sim 180$  nm gap),  $\sim 500$  nm height, and  $\sim 2^\circ$  slope angle were fabricated by interference lithography followed by a deep reactive ion etching (DRIE) (Fig. 2). Interference lithography combined with DRIE is a relatively simple and effective method for making periodic submicron scale structures over a large area with good controllability of the size and shape.<sup>39</sup> A polished silicon substrate is cleaned with a Piranha solution ( $\text{H}_2\text{SO}_4:\text{H}_2\text{O}_2$ , 3:1 in volume) and dehydrated for 10 min at 150 °C. SPR3001 photoresist (Shipley, Co.) is then spin-coated at 5000 rpm for 1 min, which gives  $\sim 50$  nm film thickness. After the spin coating, soft-bake is done at 95 °C for 1 min on a hot plate. A shadow mask made of a thin plastic film is placed over the substrate to define the desired region to be populated with nanograting structures. The substrate is then exposed under the laser interference lithography setup of “Lloyds-mirror” configuration using the He-Cd laser of the 325 nm wavelength (Nanotech, University of California, Santa Barbara) to form the nanograting pattern, followed by a postexposure bake at 115 °C for 1 min. The exposed substrate is developed by the MF701 developer (Shipley, Co.). After the development, the substrate is rinsed with deionized water and blow-dried with  $\text{N}_2$  gas followed by 1 min hard-bake at 110 °C on a hot plate. The patterned photoresist is scanned by atomic force microscope (AFM) to

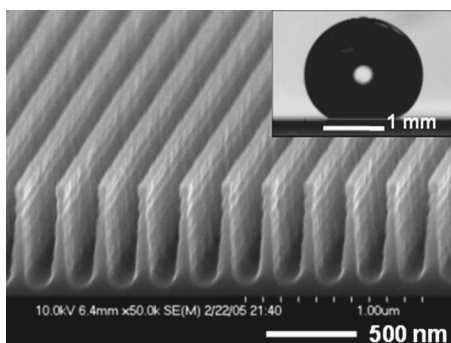


FIG. 2. Scanning electron microscopy (SEM) image of a silicon nanograting structure. The regular and well-defined nanogrates of  $\sim 230$  nm pitch (i.e., periodicity) and  $\sim 500$  nm depth, fabricated by interference lithography and deep reactive ion etching (for further details see the text and Ref. 39), uniformly cover a large area ( $2 \times 2$  cm<sup>2</sup>). The inset shows the apparent contact angle of water ( $145^\circ - 150^\circ$ ) on such a surface that is treated to be hydrophobic. Considering the ridge width ( $\sim 50$  nm) and the thickness of the Teflon hydrophobic coating ( $\sim 10$  nm), the area fraction of the liquid-solid interface on the nanograted superhydrophobic surface is  $\sim 0.3$ . The Cassie-Baxter equation (Ref. 38) also predicts an apparent contact angle of  $145^\circ - 150^\circ$  on the Teflon surface of  $\sim 0.3$  solid fraction ( $\sim 120^\circ$  on flat Teflon).

check the development. The substrate is then etched by DRIE using the patterned photoresist as an etching mask. After the DRIE, the remaining photoresist is removed and cleaned with the Piranha solution. The known fracture stress of silicon ( $\sim 2.2 \times 10^9$  Pa) assures that the high-aspect-ratio nanograting structures are robust enough to withstand most flow-induced external stresses by a large margin (e.g., the nanograting structures of aspect ratio of 10 will withstand a shear rate of more than  $10^{10}$  s<sup>-1</sup> in water flow).

### C. Fabrication of microchannels

After the nanograting structures were formed on a section of each of two silicon wafers, flow channels were created (Fig. 3). A sample has four channels (i.e., two with smooth surfaces and the other two with nanogratings) in a “+ (cross)” pattern. Fabricated on one wafer and sharing the inlet, the four channels minimize the differences amongst them. The smooth-surface channels are used as references to measure the relative increase (or decrease) of flow rate in the nanograted channels on the same sample, by which the slip lengths of the nanograted channels are obtained. One of the channels with nanogratings has the grating direction parallel to the flow, and the other transverse. The microchannels with sidewalls of  $2 - 12$   $\mu\text{m}$  in height were created on the “channel wafer” [Fig. 3(a)] by patterning a NR series photoresist (Futurrex, Inc.): NR7-3000P for  $2 - 7$   $\mu\text{m}$  and NR9-8000P for  $8 - 12$   $\mu\text{m}$ , respectively. The channel height, measured by a profilometer at more than 20 points along each channel, was uniform with standard deviation below 50 nm. The channel width is 1 mm for  $2 - 7$   $\mu\text{m}$  high channels, and 0.4 mm for  $8 - 12$   $\mu\text{m}$ . A “cover wafer” [Fig. 3(b)] has a middle inlet shared by the four microchannels, but four outer outlets, one for each channel. Reservoirs surrounding the inlet/outlets are to reduce the inlet/outlets pressure losses. The distance between two reservoirs is 4 mm, defining the length of the flow section of each channel. The inlet/outlets (

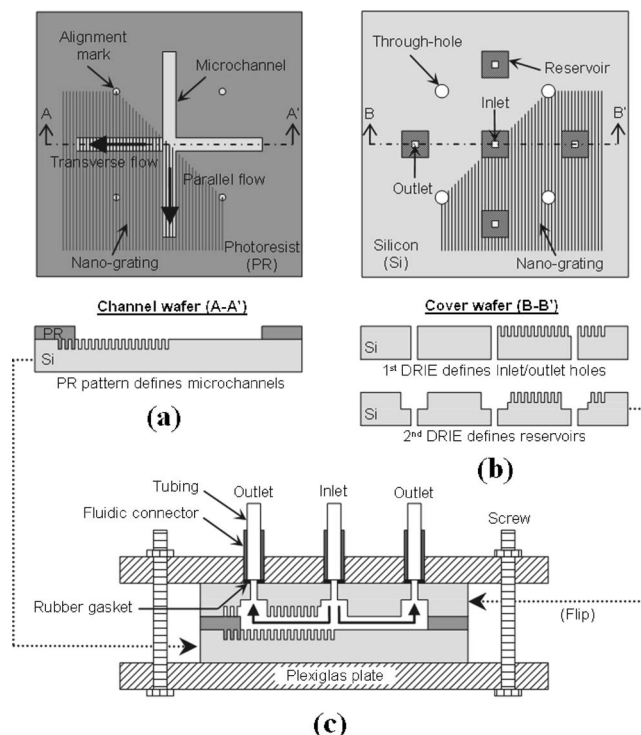


FIG. 3. Preparation of samples and flow tests. (a) Layout and fabrication of channel wafer, (b) layout and fabrication of cover wafer, (c) formation of microchannels and assembly for flow tests. For further details see the text.

$0.2 \times 0.2 \times 0.5$  mm<sup>3</sup> each) and the reservoirs ( $2 \times 2 \times 0.1$  mm<sup>3</sup> each) are fabricated by two DRIE steps using a  $\sim 20$   $\mu\text{m}$  thick photoresist (NR9-8000P) as an etch mask. The channel and the cover wafers are bonded after alignment (i.e., fitting the four alignment marks on the channel wafer into the four through-holes in the cover wafer), followed by mechanical clamping in a sample holder to reinforce the channels against deformation during pressurized flow tests [Fig. 3(c)]. The sample holder is made out of two 25 mm thick Plexiglas plates with threaded inlet/outlets in the top plate in order to connect the microchannels to a flow measurement setup. The channel surfaces can be either hydrophilic or hydrophobic. The native SiO<sub>2</sub> layer on the silicon surface is used as a hydrophilic surface. For the hydrophobic surface treatment, Teflon solution [0.2% amorphous fluoropolymer AF 1600 (DuPont) in perfluoro-compound FC-75 (Acros)] is spin-coated before the channel assembly. The advancing contact angle  $\theta_A$  of water over the Teflon coated on a smooth silicon surface was measured to be  $\sim 130^\circ$  by a goniometer. The Teflon was estimated to be  $\sim 10$  nm thick by scanning electron microscopy (SEM) pictures of the cross section of the nanograting taken before and after the coating; the same as an ellipsometer measurement on a smooth surface.

### D. Experimental approach

Using a high accuracy flow rate measurement system developed for rheometric studies in micron and submicron channels,<sup>40</sup> the slip length  $\delta$  of the nanograting surfaces is obtained by<sup>22</sup>

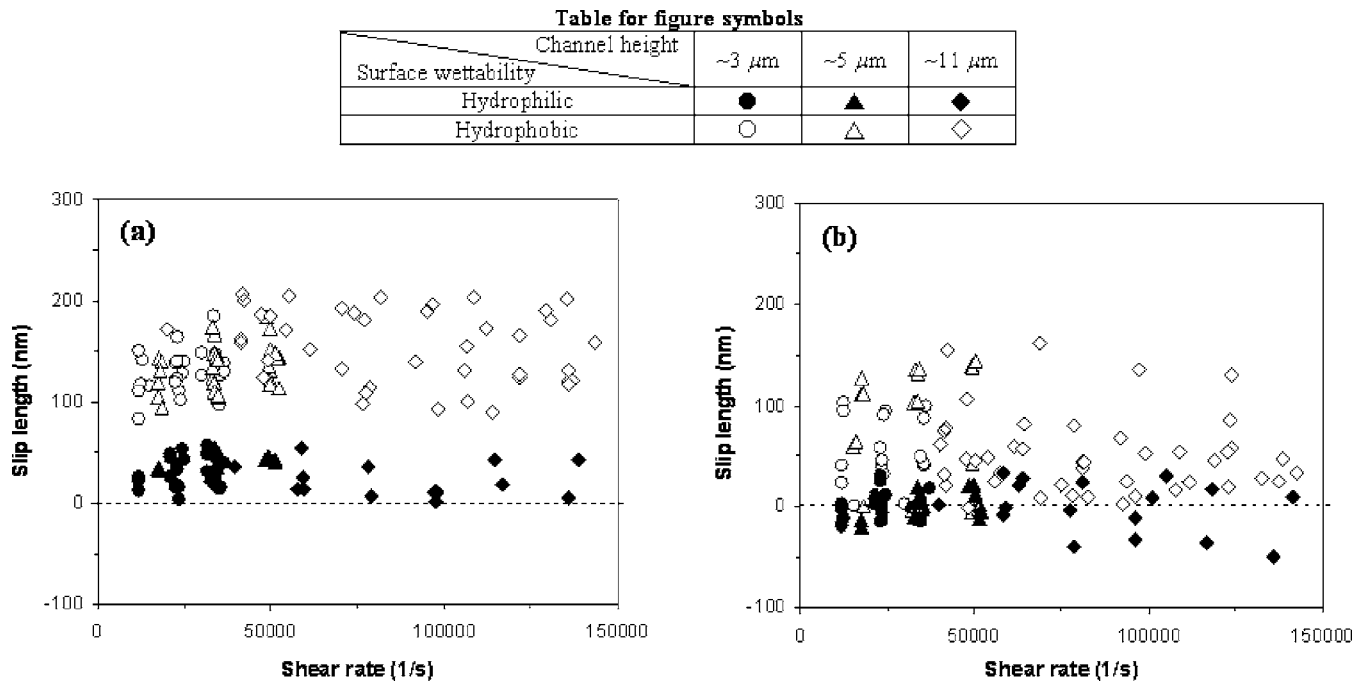


FIG. 4. Slip length of water flow over nanograting surfaces in microchannels. The slip length was obtained for a total of 24 samples. Microchannels of three different heights (i.e., 8 samples for each channel height) cover a large shear rate range. Data for hydrophobic gratings are shown with hollow patterns, hydrophilic with solid (see the table for figure symbols). (a) Flows parallel to the nanograting produced, in terms of mean and standard deviation, the slip length of  $143 \pm 35$  nm over hydrophobic nanograting and  $30 \pm 16$  nm over hydrophilic nanograting. (b) Flows transverse to the nanograting produced the slip length of  $61 \pm 44$  nm over hydrophobic nanograting and  $0 \pm 17$  nm over hydrophilic nanograting.

$$\delta = \frac{\mu QL}{2wh^2 \Delta P} - \frac{h}{3}, \quad (2)$$

where the flow rate  $Q$  of the test liquid of viscosity  $\mu$  is driven by the pressure difference  $\Delta P$  along the channel of height  $2h$ , width  $w$  ( $\gg 2h$ ), and length  $L$ . The pressure drop vs the flow rate is measured with deionized water filtered through a  $0.5 \mu\text{m}$  filter before entering the channels. For each flow measurement, only one outlet is open to test only the associated channel. The flow rate is determined by measuring the weight of the collected water on an analytical balance capable of  $\sim 1$  nL/s, compensated for the evaporation rate out of the collecting vial. The temperature of the sample is monitored on its surface by a thermocouple with accuracy of  $\pm 0.02$  °C. The temperature is used in estimating the water viscosity. The pressure difference applied to the microchannels (i.e., 0.1–1 bar) corresponds to a shear rate of  $10^4$ – $10^5$   $\text{s}^{-1}$  at the walls. After the flow reaches the stabilized steady-state at each applied pressure, the averaged flow rate over  $\sim 2$  min is selected for the experimental data.

Several samples for each channel height ranging between  $2 \mu\text{m}$  and  $12 \mu\text{m}$ , all with both hydrophilic and hydrophobic surface conditions, are tested to assure reproducibility. Since the result sensitively depends on the value of the channel height, which is considerably affected in this scale by the compression in the sample holder, our approach is to derive the height from the least-square fit to the flow rate data obtained from smooth-surface channels with the assumption of no-slip at the walls. The derived channel heights were found to be within 5% deviation from the profilometer measurement values, confirming the overall accu-

racy. The difference of the channel height between two smooth-surface channels on one wafer was found to be less than 50 nm. This confirms that the channel height is uniform over the sample and supports our approach of using the smooth-surface channel as a reference for the grated channels on the same sample. In order to make a comparison to the theoretical predictions of channel flows with a heterogeneous boundary condition on the walls,<sup>28,36</sup> the nanograting height is not included in our definition of the channel height. Thus the slip length  $\delta$  is defined as the distance from the crest of the nanograting to the depth at which the linearly extrapolated velocity reaches zero.

### III. RESULTS AND DISCUSSION

Figure 4 shows the slip length of the nanograting surfaces tested with multiple samples of  $\sim 3$ ,  $\sim 5$ , and  $\sim 11 \mu\text{m}$  high microchannels. In the case of the flow parallel to the nanogratings [Fig. 4(a)], there is a clear distinction between the hydrophilic and hydrophobic surfaces. The slip length tends to increase slightly with the shear rate in the low shear rate domain, but it stays relatively constant regardless of the channel height: a slip length of 0–60 nm ( $30 \pm 16$  nm in terms of mean and standard deviation) over the hydrophilic and 100–200 nm ( $143 \pm 35$  nm) over the hydrophobic nanograting surfaces. In the case of the flow transverse to the nanogratings [Fig. 4(b)], the distinction is not as clear, and the slip is smaller than that of parallel flow: insignificant slip ( $0 \pm 17$  nm) over the hydrophilic and 0–150 nm ( $61 \pm 44$  nm) over the hydrophobic nanograting surfaces.

Since the slip length of the nanograting surface is obtained by referencing a smooth surface with the assumption of no-slip at the walls, the absolute slip length would be slightly larger if a slip was present on the smooth surface. However, no significant slip over both the hydrophilic and hydrophobic smooth surfaces was detected under our experimental conditions, whose uncertainty level in measuring the slip length is  $\sim 30$  nm (mainly due to the inaccuracy of channel height estimation). Choi *et al.*<sup>22</sup> have already performed a similar experiment with very precise microchannels and reported a relatively small slip on the smooth surfaces (e.g., a doubtful slip on hydrophilic and  $\sim 30$  nm on hydrophobic surfaces at the shear rate of  $10^5$  s<sup>-1</sup>), assuring that such a slip, even if it exists, would be masked by the data fluctuation in the current tests. All things considered, the large slip over the hydrophobic nanograting surfaces (e.g.,  $143 \pm 35$  nm in the case of parallel flow) indicates that their effective slip was caused by the nanostrips of *air* in the grate troughs. In contrast, the water wets and fills the grate troughs in the hydrophilic condition, and the slight slip (e.g.,  $30 \pm 16$  nm in case of parallel flow) is likely caused by the nanostrips of *water* in the troughs. Since we assumed the reference plane to be located upon the top of the grates in obtaining the slip length of the nanograted surfaces, a nanograted surface should have an effective slip even if the grates are filled with water. While the hydrophilic nanogrates had almost no influence on the surface slip for transverse flow ( $0 \pm 17$  nm), they produced a measurable effective slip for parallel flow ( $30 \pm 16$  nm), confirming that nanoscale surface roughness and its pattern should be taken into account in estimating the slip effect even on hydrophilic surfaces.

Considering the minute sample-to-sample variance of the nanograte geometries and the resulting variance of the fluid fraction (i.e., the fraction of the fluid filled in the grate troughs) that may exist in our experiment, the slight deviation of the slip length result is expected. It should be noted that the range of the slip length data of the hydrophobic nanograting surfaces is relatively wider than that of the hydrophilic: in terms of the standard deviation from the mean of slip length, 35 nm vs 16 nm for the flows parallel to the nanogrates (or 44 nm vs 17 nm for the transverse). We interpret that the effective slip afforded by trapped air in a hydrophobic surface will be more sensitive to the variance than that by water in a hydrophilic surface, because air has a much lower viscosity than water. This interpretation also supports the belief that nanostrips of *air* exist in the hydrophobic grate troughs.

Note that our result was obtained under a pressurized flow condition (typically around 0.1 MPa). No apparent decrease of slip length was found over time during the experiment (typically a couple of hours long). It should also be noted that the grates are designed to be deep (i.e.,  $\sim 500$  nm) and the troughs narrow (i.e.,  $< 200$  nm), so that the effect of the meniscus sagging down into the hydrophobic troughs is negligible (i.e.,  $< 7$  nm) even at the maximum applied pressure of  $\sim 1$  bar. In other words, our nanograte surface provides an effective slip not influenced by the liquid pressure within the operating range. By comparison, a strong dependence of the slip length on the pressure was observed in the

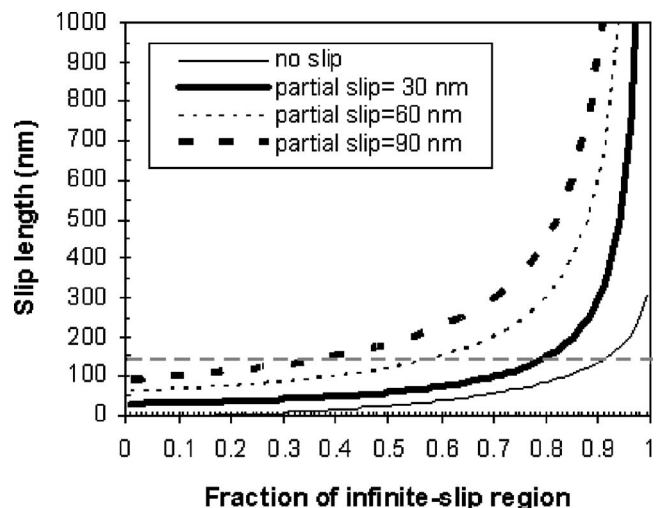


FIG. 5. Theoretically estimated slip lengths of parallel flows as a function of surface void fraction with the slip length on the solid ridge top as a parameter (0, 30, 60, or 90 nm). Since the trench of the nanograting is deep ( $\sim 500$  nm), the liquid-air interface has a large enough slip to assume an infinite slip on the void surface. The liquid-solid interface on top of the hydrophobic nanogrates, on the other hand, should have no or partial slip. The experimentally obtained mean slip length of 143 nm is added as a horizontal dotted line for comparison and further discussion in the text. For the theoretical predictions, the formula obtained with an alternating heterogeneous boundary condition of infinite-slip and partial-slip is used (Refs. 28 and 36). Note that the slip length of  $\sim 30$  nm has been reported on a flat hydrophobic surface (Ref. 22).

molecular dynamics (MD) simulations.<sup>35</sup> Although different nanopattern scales and flow conditions were studied, the dependency is apparently because the height of the grooves was so short in the MD studies (e.g., not more than ten times of the fluid molecular diameter, or a couple of nanometers) that the shape of the liquid-air interface and the corresponding air fraction are strongly affected by the liquid pressure.

Our experimental results can also be rationalized with those inferred from a macroscopic estimation,<sup>28,36</sup> where the effective slip associated with a surface characterized by a heterogeneous slip length pattern was theoretically analyzed on the basis of continuum hydrodynamics. Figure 5 shows the slip length predicted by the analytical calculations, when the flow is parallel to the alternating heterogeneous slip length pattern of infinite-slip and no or partial-slip (0, 30, 60, or 90 nm) with the fraction of infinite-slip region varied. Since the trench of our nanograting is deep ( $\sim 500$  nm) and the corresponding slip effect by the thick air is estimated to be much larger than that over the solid ridge top (e.g.,  $\sim 30$   $\mu$ m vs  $\sim 30$  nm in slip length), an infinite slip can be safely assumed at the liquid-air interface for the theoretical prediction of our experimental results. Considering the ridge width ( $\sim 50$  nm) and the thickness of Teflon hydrophobic coating ( $\sim 10$  nm), the fraction of liquid-air interface on the hydrophobic nanograted surface is  $\sim 0.7$ . If the partial slip of 30 nm reported by Choi *et al.*<sup>22</sup> is assumed on the solid ridge top of the hydrophobic nanograting, the theory predicts a slip length of 100 nm for the air fraction of 0.7, close to the mean slip length of 143 nm observed in our experiment. In light of some uncertainty in a number of factors (e.g., the slip length on the hydrophobic solid ridge surface; the fraction of air

due to the minute variation of nanograte geometries from sample to sample; potential discrepancy between theory and experiment), our experimental results agree well with the continuum hydrodynamic analysis.

Furthermore, our testing results confirm the prediction<sup>28,36,41–43</sup> that a flow transverse to the grating pattern would have a smaller effective slip than would a flow parallel to the grating. In transverse flows, the flow field near the wall constantly develops, repeatedly encountering a region of fluid over a trough and a region of solid on a grating peak; this entails a higher pressure drop overall. According to the theoretical analysis,<sup>28</sup> the effective slip length in flow transverse to the hydrophobic grating pattern is expected to be around one half of that of parallel flow, especially when the periodicity of the pattern decreases to naught. The ratio of the slip length of the transverse flow to that of the parallel flow in our experiments (Fig. 4) is 0.43 (=61/143), agreeing with the theoretical prediction. It was also reported that, in the case of transverse flow, the fraction variation of the infinite-slip region influences the overall slip more when the fraction of the infinite-slip region is near zero or near unity.<sup>28</sup> Our experimental results show that a span of slip length data for transverse flow over hydrophobic nanogratings is broader than that for the parallel flow (Fig. 4), in terms of the standard deviation from the mean slip length: 44 nm vs 35 nm. Although the difference is not so prominent mostly because of the finite air fraction (e.g., less than unity) in our nanograting pattern, if one considers the existent variation of nanograte geometries from sample to sample again, our experimental results also suggest that the effective slip is generally more sensitive to the air fraction in the case of transverse flow.

All the above details and speculations aside, it remains clear that hydrophobic nanograting surfaces demonstrate a larger effective slip than hydrophilic ones. Especially, the parallel flow over hydrophobic nanogratings shows a distinguished slip compared with the other surface and flow conditions. An important consequence of the surface slip is the reduction of drag or pressure drop, which is directly measured by the flow rate measurement in the experiment and related to the slip length by

$$\left. \frac{\Delta P_{\text{slip}}}{\Delta P_{\text{no-slip}}} \right|_Q = \left. \frac{Q_{\text{no-slip}}}{Q_{\text{slip}}} \right|_{\Delta P} = \frac{1}{1 + 3(\delta/h)}, \quad (3)$$

where the subscripts slip and no-slip denote the cases of the slip and the no-slip present at walls, respectively. Figure 6 shows the actual reduction of pressure drop measured in the case of flow parallel to the hydrophobic nanograting [shown in Fig. 4(a)]. For example, the slip length of 100–200 nm entailed a 20%–30% reduction of pressure drop in a  $\sim 3 \mu\text{m}$  high channel in our experiment. The projected reduction of pressure drop in microchannels of a different channel height  $2h$  with the slip length  $\delta$  as a parameter is also superimposed for reference, based on Eq. (3). However, it should be noted that the slip length achieved by the current nanograted superhydrophobic surface is smaller than the height of the nanograting structures, indicating that a simpler way to reduce drag or pressure drop in microchannels in practice is just to

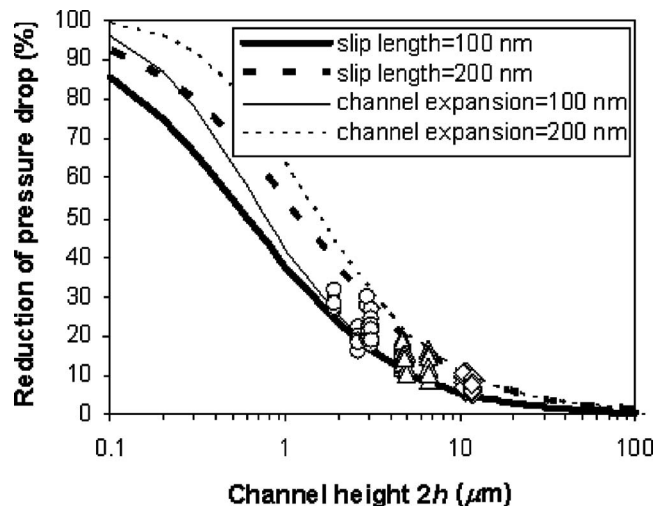


FIG. 6. Reductions of pressure drop by a nanograted superhydrophobic surface in microchannels. The slip length data for parallel flows on hydrophobic nanogrates, presented in Fig. 4(a), are converted and replotted here, keeping the same patterns ( $\circ$ ,  $\triangle$ ,  $\diamond$ ). The projected reduction of pressure drop by the surface slip as a function of channel height is drawn with thick lines (for slip length of 100 and 200 nm). For comparison and further discussion in the text, the reduction by the hypothetical channel expansion (increase of channel height at each wall by 100 and 200 nm) are drawn with thin lines.

increase the channel height as also shown in Fig. 6. However, as fabrication technology advances, the drag reduction by the effective slip can be larger than that by the simple expansion of the channel dimension, as explained next.

The slip effect will start to be insensitive to trough depths if the depth becomes larger than the period of the grooves.<sup>42</sup> Although the current nanograting trench was fabricated deeper ( $\sim 500$  nm) than necessary for a safety margin against experimental variations (e.g., pressure), trenches as shallow as  $\sim 200$  nm would provide a similar slip effect. The macroscopic analysis<sup>36</sup> (Fig. 5) predicts that a slip length greater than 200 nm is obtainable if the air fraction is greater than 0.85 with the assumption of 30 nm slip on the solid ridge top. The slip length larger than the current depth of the nanograting trench (500 nm) is further predicted when the air fraction is greater than 0.94 with 30 nm slip on the solid top (Fig. 5), which appears achievable by a new development in nanofabrication.<sup>39</sup> Furthermore, it should be noted that the slip length increases exponentially as the air fraction comes near to unity. For example, a slip length of  $3 \mu\text{m}$  is expected with the air fraction of 0.99 with 30 nm slip on the solid top, and even  $30 \mu\text{m}$  with 0.999. In prospect, the ability to tune the size and shape of the nanogrates<sup>39</sup> would enable a systematic exploration of the slip length dependence on the nanogrates' detailed geometries, such as pattern density, tip sharpness, and void fraction. Furthermore, the practical friction reduction in microfluidic systems, e.g., in microchannels would be enabled by using the well-designed nanoscale surface structures.

The *nanoscale* surface pattern, which requires a new and advanced fabrication technology, makes a difference of engineering significance. For example, the micropatterns ( $>20 \mu\text{m}$  in lateral structure size,  $>20 \mu\text{m}$  in spacing be-

tween structures, and  $>40 \mu\text{m}$  in pattern periodicity) tested by Ou and Rothenstein<sup>33,34</sup> cannot preserve the surface superhydrophobicity under highly pressurized flows and would lose its slip effect unless the flow is under a low pressure ( $<5 \text{ kPa}$ ). In contrast, the nanopatterns ( $\sim 50 \text{ nm}$  in lateral structure size,  $<200 \text{ nm}$  in spacing between structures, and  $\sim 230 \text{ nm}$  in pattern periodicity) enabled in our study can preserve the surface superhydrophobicity even under highly pressurized flow (up to  $\sim 500 \text{ kPa}$ , 100 times greater than that of Ou and Rothenstein's micropatterns). Although the practical friction reduction by using nanostructured superhydrophobic surface has been proposed theoretically and numerically,<sup>35,36</sup> the inability to realize regular and well-controlled nanostructures over a large pattern area has hindered experimental verification. In this regard, our study is the *first* experimental approach to examine the effect of a regular *nanoscale* surface pattern, which is not readily obtainable by a conventional micromachining technology, on the liquid slip. Furthermore, our nanostructured surface pattern is more relevant to innate surface roughness so that our study can lead further to the systematic elucidation of the effect of nanoscale surface roughness upon the liquid slip, including nanobubble effects.

While the flow in microchannels tested in this study was laminar, the measurable and directional slip effect of the nanograting surface remains important for turbulent flows. The slip effect on flow stability, transition to turbulence, and overall drag reduction in macroscale flows is also of great interest for many engineering applications—naval in particular. A numerical study<sup>44</sup> suggested that a significant drag reduction could be achieved in large-scale flows if a surface has a slip length on the order of several wall units. The numerical study showed that the skin-friction drag was reduced with a streamwise slip, while the opposite effect was seen with a spanwise slip. It was further shown that the transition to turbulence was delayed significantly with a streamwise slip, whereas a spanwise slip induces an earlier transition.<sup>45</sup> A series of wind-tunnel experiments<sup>46</sup> further reported that relatively small changes in the arrangement of specified patterns of protrusions in walls could alter the response of the system from drag reduction to drag enhancement in turbulent channel flow. These imply that a surface with specified directional sensitivity is desired. Our results suggest that the directional control of a slip is possible by the design of the nanostructure patterns on the surface. By aligning nanostructures into directional patterns, a hydrophobic surface with a large slip in one direction and a minimum slip in another direction can be envisioned in order to achieve the maximum benefits.

Although the effective slip is commonly considered for friction reduction of liquid including microchannel flows, its utility is much wider. For instance, the large effective slip can help flatten the velocity profiles within microchannels, which can be utilized to reduce the dispersion in microfluidic separation systems.

## IV. CONCLUSIONS

By using a previously unavailable technique to fabricate densely populated tall nanostructures over a large area, we designed well-defined, nanoperiodic deep grating patterns and experimentally studied the effect of nanoscale surface features (or structures) on a liquid slip and a corresponding friction reduction in microchannels. That the large effective slip lengths obtained over the nanograted superhydrophobic surface are in quantitative agreement with analytical predictions supports the idea that nanostrips of air exist in the hydrophobic nanograte troughs and persist even under pressurized flows. In addition, we confirmed experimentally that the flows parallel to the nanograting pattern experience a larger effective slip than the transverse flows do.

Although the slip effect by nanoscale features with varying surface wettability is of fundamental importance to the physics of fluids, our main goal is to develop slip surfaces of engineering significance (i.e., useful in practice). Such surfaces should allow a large effective slip even under pressurized flow conditions. Although the flow tests in this paper were done in microchannels, applications are also likely at the macroscopic level, e.g., high-Reynolds-number underwater vehicles. While surface structures with *microscale* periodicity may provide a similarly large slip effect under experimental conditions with limited pressure, those with *nanoscale* features enable real engineering applications as demonstrated here for high pressure flows.

In conclusion, the control of boundary slip on structured superhydrophobic surfaces is not only of scientific interest but also can be of practical use for engineering problems, including microfluidic systems, when the surface structures are designed appropriately for the purpose. Recent advancement in nanotechnology has played a key role in enabling such structures.

## ACKNOWLEDGMENTS

This work has been supported by the NSF NIRT Grant No. 0103562. The authors thank the Nanotech in the University of California, Santa Barbara (UCSB) for the use of interference lithography setup, and Professor Robin L. Garrell and Professor Fred Wudl at UCLA for their constructive advice as this work has evolved. We also appreciate valuable discussions of numerical predictions with Professor Carl Meinhart and Dr. Xioajun Liu at UCSB.

<sup>1</sup>J. Koplik, J. R. Banavar, and J. F. Willemsen, "Molecular dynamics of fluid flow at solid surfaces," *Phys. Fluids A* **1**, 781 (1989).

<sup>2</sup>M. Cieplak, J. Koplik, and J. R. Banavar, "Boundary conditions at a fluid-solid interface," *Phys. Rev. Lett.* **86**, 803 (2001).

<sup>3</sup>M. Sun and C. Ebner, "Molecular dynamics study of flow at a fluid-wall interface," *Phys. Rev. Lett.* **69**, 3491 (1992).

<sup>4</sup>P. A. Thompson and S. M. Troian, "A general boundary condition for liquid flow at solid surfaces," *Nature (London)* **389**, 360 (1997).

<sup>5</sup>S. Granick, Y. Zhu, and H. Lee, "Slippery questions about complex fluids flowing past solids," *Nat. Mater.* **2**, 221 (2003).

<sup>6</sup>C. Neto, D. R. Evans, E. Bonaccorso, H.-J. Butt, and V. S. J. Craig, "Boundary slip in Newtonian liquids: A review of experimental studies," *Rep. Prog. Phys.* **68**, 2859 (2005).

<sup>7</sup>E. Lauga, M. P. Brenner, and H. A. Stone, "Microfluidics: The no-slip boundary condition," in *Handbook of Experimental Fluid Dynamics* (Springer, New York, 2005), Chap. 15.

- <sup>8</sup>E. Bonaccorso, M. Kappl, and H.-J. Butt, "Hydrodynamic force measurement: Boundary slip of water on hydrophilic surfaces and electrokinetic effects," *Phys. Rev. Lett.* **88**, 076103 (2002).
- <sup>9</sup>E. Bonaccorso, H.-J. Butt, and V. S. J. Craig, "Surface roughness and hydrodynamic boundary slip of a Newtonian fluid in a completely wetting system," *Phys. Rev. Lett.* **90**, 144501 (2003).
- <sup>10</sup>T. D. Blake, "Slip between a liquid and a solid: D. M. Tolstoy's (1952) theory reconsidered," *Colloids Surf.* **47**, 135 (1990).
- <sup>11</sup>O. I. Vinogradova, "Drainage of a thin liquid film confined between hydrophobic surfaces," *Langmuir* **11**, 2213 (1995).
- <sup>12</sup>E. Schnell, "Slippage of water over nonwettable surfaces," *J. Appl. Phys.* **27**, 1149 (1956).
- <sup>13</sup>E. Ruckenstein, and P. Rajora, "On the no-slip boundary condition of hydrodynamics," *J. Colloid Interface Sci.* **96**, 488 (1983).
- <sup>14</sup>N. V. Churaev, V. D. Sobolev, and A. N. Somov, "Slippage of liquids over lyophobic solid surfaces," *J. Colloid Interface Sci.* **97**, 574 (1984).
- <sup>15</sup>O. I. Vinogradova, "Slippage of water over hydrophobic surfaces," *Int. J. Min. Process.* **56**, 31 (1999).
- <sup>16</sup>R. Pit, H. Hervet, and L. Leger, "Direct experimental evidence of slip in hexadecane-solid interfaces," *Phys. Rev. Lett.* **85**, 980 (2000).
- <sup>17</sup>Y. Zhu and S. Granick, "Rate-dependent slip of Newtonian liquid at smooth surfaces," *Phys. Rev. Lett.* **87**, 096105 (2001).
- <sup>18</sup>Y. Zhu and S. Granick, "Limits of the hydrodynamic no-slip boundary condition," *Phys. Rev. Lett.* **88**, 106102 (2002).
- <sup>19</sup>J. Baudry, E. Charlaix, A. Tonck, and D. Mazuyer, "Experimental evidence for a large slip effect at a nonwetting fluid-solid interface," *Langmuir* **17**, 5232 (2001).
- <sup>20</sup>C. Cottin-Bizonne, S. Jurine, J. Baudry, J. Crassous, F. Restagno, and E. Charlaix, "Nanorheology: An investigation of the boundary condition at hydrophobic and hydrophilic interfaces," *Eur. Phys. J. E* **9**, 47 (2002).
- <sup>21</sup>D. Trethewey and C. Meinhart, "Apparent fluid slip at hydrophobic microchannel walls," *Phys. Fluids* **14**, L9 (2002).
- <sup>22</sup>C.-H. Choi, K. J. A. Westin, and K. S. Breuer, "Apparent slip flows in hydrophilic and hydrophobic microchannels," *Phys. Fluids* **15**, 2897 (2003).
- <sup>23</sup>J.-H. Cho, B. M. Law, and F. Rieutord, "Dipole-dependent slip of Newtonian liquids at smooth solid hydrophobic surfaces," *Phys. Rev. Lett.* **92**, 166102 (2004).
- <sup>24</sup>J.-L. Barrat and L. Bocquet, "Large slip effect at a nonwetting fluid-solid interface," *Phys. Rev. Lett.* **82**, 4671 (1999).
- <sup>25</sup>N. Ishida, T. Inoue, M. Miyahara, and K. Higashitani, "Nano bubbles on a hydrophobic surface in water observed by tapping-mode atomic force microscopy," *Langmuir* **16**, 6377 (2000).
- <sup>26</sup>J. W. G. Tyrrell and P. Attard, "Images of nanobubbles on hydrophobic surfaces and their interactions," *Phys. Rev. Lett.* **87**, 176104 (2001).
- <sup>27</sup>P. G. de Gennes, "On fluid/wall slippage," *Langmuir* **18**, 3413 (2002).
- <sup>28</sup>E. Lauga and H. A. Stone, "Effective slip in pressure-driven Stokes flow," *J. Fluid Mech.* **489**, 55 (2003).
- <sup>29</sup>D. Trethewey and C. Meinhart, "A generating mechanism for apparent fluid slip in hydrophobic microchannels," *Phys. Fluids* **16**, 1509 (2004).
- <sup>30</sup>K. Watanabe, Y. Udagawa, and H. Udagawa, "Drag reduction of Newtonian fluid in a circular pipe with highly water-repellent wall," *J. Fluid Mech.* **381**, 225 (1999).
- <sup>31</sup>K. Watanabe, T. Takayama, S. Ogata, and S. Isozaki, "Flow between two coaxial rotating cylinders with a highly water-repellent wall," *AIChE J.* **49**, 1956 (2003).
- <sup>32</sup>S. Gogte, P. Vorobieff, R. Truesdell, A. Mammoli, F. V. Swol, P. Shah, and C. J. Brinker, "Effective slip on textured superhydrophobic surfaces," *Phys. Fluids* **17**, 051701 (2005).
- <sup>33</sup>J. Ou, B. Perot, and J. P. Rothstein, "Laminar drag reduction in microchannels using ultrahydrophobic surfaces," *Phys. Fluids* **16**, 4635 (2004).
- <sup>34</sup>J. Ou and J. P. Rothstein, "Direct velocity measurements of the flow past drag-reducing ultrahydrophobic surfaces," *Phys. Fluids* **17**, 103606 (2005).
- <sup>35</sup>C. Cottin-Bizonne, J.-L. Barrat, L. Bocquet, and E. Charlaix, "Low-friction flows of liquid at nanopatterned interfaces," *Nat. Mater.* **2**, 237 (2003).
- <sup>36</sup>C. Cottin-Bizonne, C. Barentin, E. Charlaix, L. Bocquet, and J.-L. Barrat, "Dynamics of simple liquids at heterogeneous surfaces: Molecular-dynamics simulations and hydrodynamic description," *Eur. Phys. J. E* **15**, 427 (2004).
- <sup>37</sup>C.-H. Choi and C.-J. Kim, "Large slip of aqueous liquid flow over a nanoengineered superhydrophobic surface," *Phys. Rev. Lett.* **96**, 066001 (2006).
- <sup>38</sup>J. Kim and C.-J. Kim, "Nanostructured surface for dramatic reduction of flow resistance in droplet-based microfluidics," in *Proceedings of the 15th IEEE International Conference on Micro Electro Mechanical Systems*, Las Vegas, Nevada (IEEE, Piscataway, 2002), pp. 479–482.
- <sup>39</sup>C.-H. Choi and C.-J. Kim, "Fabrication of silicon nanostructures with various sidewall profiles and sharp tips," in *Proceedings of the 13th International Conference on Solid-State Sensors, Actuators and Microsystems*, Seoul, Korea (IEEE, Piscataway, 2005), pp. 168–171.
- <sup>40</sup>U. Ulmanella, "Molecular effects on the boundary condition in micro and nano fluidic channels," Ph.D. dissertation, Biomedical Engineering Department, University of California, Los Angeles, 2003.
- <sup>41</sup>P. Luchini, F. Manzo, and A. Pozzi, "Resistance of a grooved surface to parallel flow and cross-flow," *J. Fluid Mech.* **228**, 87 (1991).
- <sup>42</sup>C. Y. Wang, "Flow over a surface with parallel grooves," *Phys. Fluids* **15**, 1114 (2003).
- <sup>43</sup>N. V. Priezjev, A. A. Darhuber, and S. M. Troian, "Slip behavior in liquid films on surfaces of patterned wettability: Comparison between continuum and molecular dynamics simulations," *Phys. Rev. E* **71**, 041608 (2005).
- <sup>44</sup>T. Min and J. Kim, "Effects of hydrophobic surface on skin-friction drag," *Phys. Fluids* **16**, L55 (2004).
- <sup>45</sup>T. Min and J. Kim, "Effects of hydrophobic surface on stability and transition," *Phys. Fluids* **17**, 108106 (2005).
- <sup>46</sup>L. Sirovich and S. Karlsson, "Turbulent drag reduction by passive mechanisms," *Nature (London)* **388**, 753 (1997).